Journal of Statistical Physics, Vol. 107, Nos. 1/2, April 2002 (© 2002)

Shear Stress in a Couette Flow of Liquid-Particle Suspensions

A. Shakib-Manesh,[1,2] P. Raiskinmäki,[1] A. Koponen,[1] M. Kataja,[1] and J. Timonen[1]

Received February 16, 2001; accepted November 19, 2001

The mechanisms of momentum transfer and shear stress of liquid-particle suspensions in two-dimensional Couette flow are studied using direct numerical simulation by lattice-Boltzmann techniques. The results obtained display complex flow phenomena that arise from the two-phase nature of the fluid including a nonlinear velocity profile, layering of particles, and apparent slip near the solid walls. The general rheological behaviour of the suspension is dilatant. A detailed study of the various momentum transfer mechanisms that contribute to the total shear stress indicates that the observed shear thickening is related to enhanced relative solid phase stress for increasing shear rates.

KEY WORDS: Suspension; lattice-Boltzmann; momentum transfer; shear stress.

1. INTRODUCTION

The flow dynamics of dense liquid-particle suspensions is of great fundamental and practical interest. Such a suspension may have a complicated mesoscopic structure that often manifests itself in the macroscopic scale as an intricate flow behaviour (here "mesoscopic" refers to the typical size and time scales of the suspended particles). In practice, the underlying two-phase character is often neglected, and the suspension is treated as a non-Newtonian fluid. This problem has also been studied previously,[1–3] but no satisfactory description of the rheological response, particularly for concentrated dispersions, has emerged. The most simple, yet a widely used approach then is to adopt the classical viscosity assumption whereby the stress tensor is proportional to the strain-rate tensor. The coefficient of

[1] Department of Physics, University of Jyväskylä, P.O. Box 35 (YFL), FIN-40351 Jyväskylä, Finland.

[2] To whom correspondence should be addressed; e-mail: Amir@phys.jyu.fi

0022-4715/02/0400-0067/0 © 2002 Plenum Publishing Corporation

proportionality, the dynamic viscosity of the suspension, may depend on flow conditions and on various material properties such as the volume fraction of suspended particles, particle shape, size distribution, particle–particle interactions, and on the properties of the suspending liquid.

While such an approach may be useful for dilute, homogeneous, isotropic suspensions with small particles of regular shape, it is mostly inadequate for dense suspensions found in many practical flow problems. The reasons for this are readily understood at a qualitative level. In a laminar flow of a typical single-phase fluid, the internal "extra stress" (i.e., the stress in excess of the isotropic pressure) arises from molecular interactions and the related random motions. This additional stress is adequately described by the usual concept of viscosity. In addition to the viscous stress in the fluid phase, also other mechanisms exist for momentum transport in liquid-particle suspensions. These mechanisms include particle–particle collisions and stress inside the particles. Both the fluid and the particles also undergo random motions that arise from the presence of particles, and it appears even in the case when the flow is laminar in the mesoscopic scale.[4] This "pseudo-turbulent" motion may give rise to additional stress in analogy with Reynolds stress in conventional turbulent flow. Complicated phenomena such as clustering and layering of particles may occur, and particles may migrate into and accumulate in some part of the system.[5, 6] In particular, particles may move away from the solid walls thus creating a particle-free "lubrication layer."[7] In a typical viscometric measurement, bulk quantities such as the total flux, mean shear rate, pressure drop and total shear stress are measured. Extracting the relevant rheological parameters from the measured results usually requires making specific assumptions concerning the actual state of the flow in the device.[3] Complicated collective effects can make the two-phase flow non-homogeneous or non-isotropic (homogeneity and isotropy are both implicit assumptions in the classical viscosity hypothesis), and thereby cause, e.g., the mean flow profile to deviate from the assumed profile, and thus lead to misinterpretation of data.

In general, measuring of the local instantaneous flow quantities such as velocities and stresses, separately for both phases, is not feasible in a dense liquid-particle suspension. It is practically impossible to measure, e.g., the particulate stress, apart from the total stress, needed for finding experimental correlations that would truly appreciate the two-phase character of the suspension and reveal complicated mesoscopic phenomena, such as the effect of inertia on the interaction of two solid particles.[8] In principle, such information can be attained from results of direct numerical simulations of the flow. Such results are however subject to uncertainties that arise from the flow model, and from the numerical techniques used. Yet, useful qualitative information about the relevant mesoscopic processes that contribute, e.g.,

to the macroscopic shear stress measured in a viscometer, can be obtained using direct simulations.

In this work we use direct numerical simulations to qualitatively analyze the basic mechanisms that contribute to the total shear stress in a simple two-dimensional Couette flow of a monodisperse liquid-particle suspension. To this end we utilize the lattice-Boltzmann scheme that is a recently developed technique for modeling various transport phenomena. The algorithm is based on discretized kinetic theory, and is quite simple to apply and use. There has been considerable progress recently in the development of lattice-Boltzmann methods.[9] The applications of the technique range from crack and wave propagation[10, 11] to diffusion and quantum mechanics,[12, 13] but fluid-flow problems have been the most important area of application of the method. Indeed, several physically plausible models have been developed for complicated flows such as those of multiphase and multicomponent fluids,[14, 15] non-Newtonian and compressible fluids,[16, 17] and suspensions.[18, 19] Within the present application, the flow of the carrier liquid is solved using the lattice-Boltzmann method while the motion of the cylindrical particles suspended in the fluid is governed by Newtonian mechanics.

Using the detailed time-dependent numerical solution of the two-dimensional Couette flow for the carrier fluid, and for the suspended particles, we compute the time-averaged total shear stress and the mean velocity profile of the suspension, and study the distribution of particles in the flow field. We demonstrate the existence of a nonlinear velocity profile and collective phenomena such as layering of particles, and discuss their effects on the apparent viscosity of the suspension, as can be measured in an appropriate viscometric experiment.

To understand the underlying mesoscopic mechanisms that contribute to the total observable shear stress (and apparent viscosity), we compute the stresses of different phases and momentum fluxes, including the viscous stress in the fluid phase, the structural stress inside the particles, and the inertial fluxes that arise from the pseudo-turbulent fluctuations of both phases. The mean shear stress inside each individual particle is calculated indirectly from the hydrodynamic forces that act on the surface of the particle. Notice also that since the lattice-Boltzmann method is not based on the conventional continuity and Navier–Stokes equations, but on a discretized Boltzmann equation, evaluation of, e.g., hydrodynamic forces acting on particles and stresses for the fluid phase can be done without reference to the averaged fluid-dynamical quantities such as the viscous stress tensor.[20]

As we concentrate here on the basic mechanisms that are responsible for the solid volume fraction and Reynolds number dependence of viscosity, we

only consider the zero-gravity situation. In an experimental system gravity may or may not be important, and one has to pay attention to this problem.

2. THE LATTICE-BOLTZMANN METHOD FOR SUSPENSION SIMULATIONS

The key idea behind the lattice-Boltzmann models of fluids is to solve a discretized Boltzmann equation on a regular lattice where the fluid is modeled with particle distributions.[21] At every time step, each fluid particle propagates to a neighbouring lattice point and undergoes local collisions in which the momenta are redistributed. In the present 2D simulations we have used a square lattice where particles can either move to the nearest or the next-nearest neighbours, or remain at rest.

There are several different lattice-Boltzmann models for Newtonian incompressible fluids. In this work we use the so-called lattice-BGK model. The dynamics of this model is given by the equation[22, 23]

$$f_i(\mathbf{r}+\mathbf{c}_i, t+1) = f_i(\mathbf{r}, t)+\frac{1}{\tau}[f_i^{\mathrm{eq}}(\mathbf{r}, t)-f_i(\mathbf{r}, t)] \tag{1}$$

where $\mathbf{c}_i$ is a vector pointing to a neighbouring lattice node, $f_i(\mathbf{r}, t)$ is the density of the fluid particles moving in the $\mathbf{c}_i$ direction, τ is the BGK relaxation parameter, and $f_i^{\mathrm{eq}}(\mathbf{r}, t)$ is the equilibrium distribution towards which the particle populations are relaxed.

The basic hydrodynamic variables are obtained in the lattice-Boltzmann model from the velocity moments in analogy with the kinetic theory of gases. The density ρ and the flow velocity $\mathbf{u}$ of the fluid are given by

$$\rho(\mathbf{r}, t) = \sum_{i=1}^{N} f_i(\mathbf{r}, t) \tag{2}$$

and

$$\rho(\mathbf{r}, t)\,\mathbf{u}(\mathbf{r}, t) = \sum_{i=1}^{N} \mathbf{v}_i f_i(\mathbf{r}, t) \tag{3}$$

Here $\mathbf{v}_i$ is the velocity of the particle population f_i, and N is the total number of different fluid particles. A common choice for the equilibrium distribution is

$$f_i^{\mathrm{eq}}(\rho, \mathbf{u}) = \rho t_i \left(1+\frac{1}{c_s^2}(\mathbf{c}_i\cdot\mathbf{u})+\frac{1}{2c_s^4}(\mathbf{c}_i\cdot\mathbf{u})^2-\frac{1}{2c_s^2}u^2\right) \tag{4}$$

where t_i is a weight factor that depends on the length of the link vector $\mathbf{c}_i$, and c_s is the speed of sound in the fluid. The weight factors t_i, and thus the speed of sound c_s, can be chosen in different ways. The kinematic viscosity of the simulated fluid is given by $\nu = (2\tau - 1)/6$ (in lattice units).[22] The fluid pressure can be expressed in the form

$$p(\mathbf{r}, t) = c_s^2 \, \Delta\rho(\mathbf{r}, t) = c_s^2(\rho(\mathbf{r}, t) - \rho_f) \tag{5}$$

where ρ_f is the average density of the fluid.

The fluid momentum tensor $\mathbf{\Pi}_f$ can be obtained from the pre-collision and post-collision populations f_i and f_i^* by

$$\Pi_f^{\alpha\beta}(\mathbf{r}, t) = \tfrac{1}{2} \sum_{i=1}^{N} v_{i\alpha} v_{i\beta} f_i(\mathbf{r}, t) + \tfrac{1}{2} \sum_{i=1}^{N} v_{i\alpha} v_{i\beta} f_i^*(\mathbf{r}, t) \tag{6}$$

The convection tensor for each phase (α),

$$\mathbf{C}_\alpha = \rho_\alpha \mathbf{u}\mathbf{u} \tag{7}$$

can directly be calculated from density ρ and velocity $\mathbf{u}$, and the viscous stress tensor $\mathbf{\Sigma}_f$ is given by

$$\mathbf{\Sigma}_f = \mathbf{\Pi}_f - \mathbf{C}_f \tag{8}$$

Solid obstacles such as suspended particles are included in the lattice-Boltzmann model by using their discrete images. The lattice points that are located inside a particle are assumed to belong to that particle. There are two different lattice points of this kind, the interior points and the boundary points. Each boundary point has at least one link $\mathbf{c}_i$ pointing to the fluid phase.

The no-slip boundary condition at solid-fluid interfaces is usually realized in lattice-Boltzmann simulations through a simple bounce-back condition, where the momenta of the fluid particles are reversed at the boundary points. The bounce-back condition can be generalized to moving boundaries, whereby the particle distributions are modified at boundary points according to[24]

$$f_i(\mathbf{r} + \mathbf{c}_i, t+1) = f_{i'}(\mathbf{r} + \mathbf{c}_i, t_+) + 2\rho_f B_i(\mathbf{u}_w \cdot \mathbf{c}_i) \tag{9}$$

Here t_+ indicates the time right after the collision, i' denotes the bounce-back link, coefficients B_i depend on the equilibrium distribution f^{eq}, and $\mathbf{u}_w$ is the wall velocity. The last term in Eq. (9) accounts for the momentum transfer between the fluid and the moving solid wall.

Several lattice-Boltzmann models for suspensions have been developed.[18, 25–27] Here, we use the model of ref. 26, where the fluid covers the entire lattice, and the lattice-Boltzmann collision operation is applied at every lattice node including the boundary and interior points of the particles. In this model a solid particle consists of a solid matrix, and of an interior fluid that is called the fluid core of the particle. The mass M_s of the solid matrix is distributed uniformly in the interior and boundary points giving a density ρ_s for the solid matrix. However, the solid matrix interacts with the fluid phase and with the core fluid only at the boundary points. The total hydrodynamic force and torque acting on the solid matrix can be obtained at each time step by summing the effect of Eq. (9) at all boundary points. The solid matrix can then be moved according to normal Newtonian dynamics. Notice that the fluid core increases the effective mass and the effective moment of inertia of the suspended particles. The effective density of the particle is $\rho_p = \rho_s + \rho_f$.

As has been shown in refs. 24–26, 28, the lubrication forces given by the lattice-Boltzmann model may be too small when particles are very close to each other. This could be avoided by adding explicit lubrication forces between the particles (see ref. 29). Here we simply allow elastic frictionless collisions between the solid matrices when particles touch each other. Taking into account the effect of the core fluid, the collision of two particles is highly dissipative. The lubrication forces, which are properly accounted for by the lattice-Boltzmann model at distances larger than one lattice spacing, are however strong enough to keep the particles separated most of the time. In the present 2D simulations, the contribution of direct collisions is thus negligible (always less than 0.5% of the total stress). In order to find however if dissipative particle–particle collisions have a significant effect on the behaviour of viscosity, we also analyzed the model in which these collisions are elastic (by forcing the core fluid to have the appropriate momentum transfer in the collision). We found that the difference in viscosity and shear stress resulting from the collision mechanism was less than 5% for the Reynolds numbers and solid volume fractions considered here. Therefore we only give the results for the dissipative collisions. Also, the simulations are done in the kinetic regime where Brownian motion of the suspended particles can be neglected.[30]

The lattice-Boltzmann suspension model used here is computationally very convenient, as there is no need to create and destroy fluid when the suspended particles move. The method can be efficiently implemented on parallel processors, and the particle-particle interactions, the flow geometry, the Peclet number, the shear rate and shear Reynolds number, as well as the size and shape of the suspended particles can easily be varied. One restriction of the model is that the particle density ρ_p must be clearly higher

than the fluid density ρ_f in order to avoid numerical instabilities. The inertial effects of the filling fluid may also decrease the accuracy of this method,[8, 27] and can add extra dissipation in collisions between the suspended particles. Notice that these difficulties do not arise in those implementations of the lattice-Boltzmann method in which particles have an all solid core.[18, 8]

For $2 \lesssim \rho_p/\rho_f \lesssim 5$, e.g., we find however that the actual density ratio does not affect much the viscosity or the relevant momentum transfer ratios for the Reynolds numbers and solid volume fractions we consider here, the results obtained for different density ratios being within a few percent from each others. Beyond $\rho_p/\rho_f \approx 5$ inertial effects begin to appreciably show up for the highest Reynolds numbers, which is to be expected. In addition, benchmark tests reported in refs. 25–28 indicate that the method applied here is adequate for realistic suspension simulations. In order to lend further support to this conclusion, we also carried out the lateral migration test of refs. 18 and 31, and found[32] that a particle initially placed near a wall will migrate to the middle of the channel in good agreement with the results of refs. 18 and 31.

3. MOMENTUM TRANSPORT AND STRESS

The total momentum flux $\mathbf{F}$ through any surface S is given by

$$\mathbf{F} = \int_S \mathbf{\Pi} \cdot d\mathbf{S} \tag{10}$$

where $\mathbf{\Pi}$ is the total momentum tensor. In the present case it can be written as

$$\mathbf{\Pi} = \mathbf{C}_f + \mathbf{C}_s + \mathbf{\Sigma}_f + \mathbf{\Sigma}_s \tag{11}$$

where $\mathbf{C}_f$ and $\mathbf{C}_s$ are the convective momentum tensors, and $\mathbf{\Sigma}_f$ and $\mathbf{\Sigma}_s$ are the internal stress tensors for the fluid and the solid phase, respectively. A schematic illustration of the simulation setup together with a snapshot of an actual solution for the Couette flow of the suspension is shown in Fig. 1. In this figure the surface $S = S(y)$ is a plane perpendicular to the y axis. The total shear stress acting on this plane is defined by

$$\tau_T = \sigma_f + \sigma_s + \tau_f + \tau_s \tag{12}$$

$$\equiv \langle C_f^{xy} \rangle + \langle C_s^{xy} \rangle + \langle \Sigma_f^{xy} \rangle + \langle \Sigma_s^{xy} \rangle \tag{13}$$

where $\langle\ \rangle$ denotes averaging over space, time and ensemble. Here we calculate all averaged quantities in a macroscopically stationary state and,

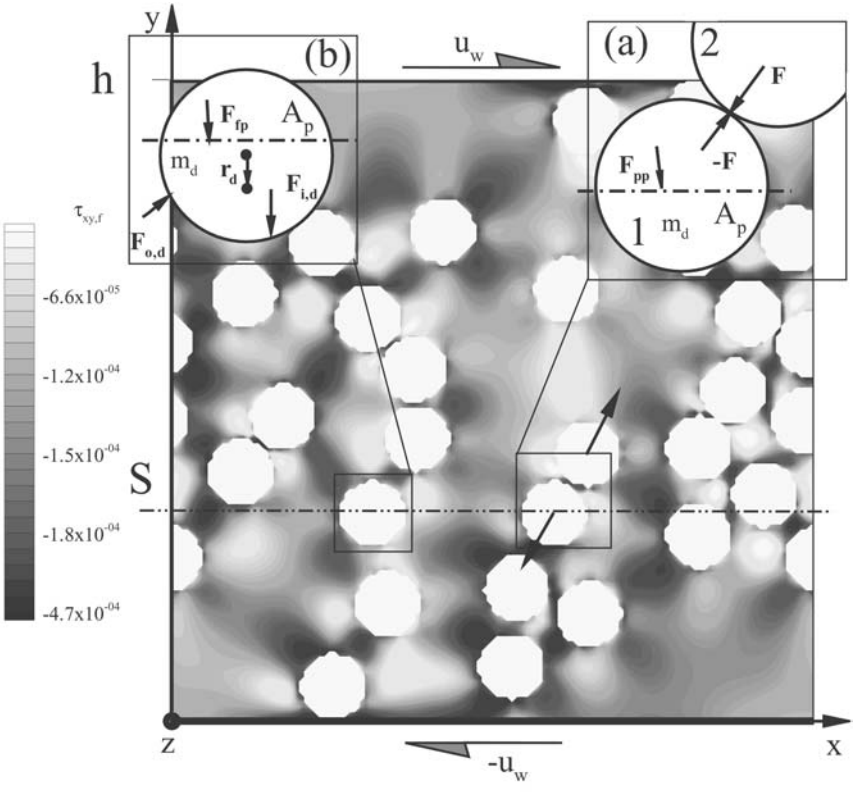

Fig. 1. A snapshot of a two-dimensional Couette-flow of liquid-particle suspension solved by the lattice-Boltzmann method. Colour coding indicates viscous shear stress in the fluid phase. The two insets show the forces used in calculating the internal particle stress due to collisions (a) and due to hydrodynamic forces (b).

assuming ergodicity, perform averaging over a long period of time, over volume or surface, and over a number of macroscopically identical systems. Stresses σ_f and σ_s contain the stresses due to pseudo-turbulent motion of the two phases, τ_f contains the viscous stress of the fluid phase and τ_s contains the internal stress of particles (and corresponds to the elastic stress of physical solid particles).

Stresses σ_f, τ_f and σ_s can all be directly calculated for each lattice point using Eqs. (6)–(8). Notice that in σ_s both the convection of the solid matrix and the convection of the fluid core have to be included. Notice also that the convection and stress of fluid at the boundary points of the particles are included in σ_f and τ_f, respectively.

Evaluation of the actual stress distribution inside solid particles would require solving, separately for each suspended particle, the time-dependent elastic continuum equations with boundary conditions given by the hydrodynamic forces due to the surrounding fluid, and the impulsive forces due to particle–particle collisions. Fortunately, it is not necessary to carry out here this formidable numerical effort. It is well known[33] that the mean value of stress inside a solid body is determined by the forces acting on the surface of the body, and is not affected by the elastic properties of the solid material. Thus, given the motion of the particle and the forces acting on its surface, one can obtain the mean stress inside the particle by a consistent use of the present model (where "particle" is constructed of a solid matrix and a core fluid), and the result will equal the mean stress in a physical solid particle in the same kinetic state. The stress τ_s can thus be written in the form

$$\tau_s = \tau_c + \tau_{pp} + \tau_{fp} \tag{14}$$

where τ_c is the stress in the core fluid while τ_{pp} and τ_{fp} are the stresses in the solid matrix caused by particle–particle collisions and by interactions between the fluid and the particle, respectively. The stress τ_c can be obtained directly from Eq. (8). In order to calculate stresses τ_{pp} and τ_{fp} we consider an impulsive force $\mathbf{F}_{pp}$ due to the particle–particle collisions and a force $\mathbf{F}_{fp}$ due to the hydrodynamic interactions that both act on a surface A_p that is formed by intersection of surface S and the particle (see the insets in Fig. 1). Since the collisions are assumed frictionless and the particles are circular and smooth, the angular velocity does not change in a collision. It is then easy to show that the collisional force on A_p can be written as

$$\mathbf{F}_{pp} = \frac{m_d \, \Delta\mathbf{p}}{M_s \, \Delta t} \tag{15}$$

where Δt is the collision time (1 in lattice units), M_s is the total mass of the solid matrix of the particle, m_d is the mass of the lower part of the particle, and $\Delta\mathbf{p}$ is the total momentum change of the particle due to collision (see inset (a) in Fig. 1). In simulations, mass m_d can simply be calculated by counting the number of lattice points that are located below the plane S inside the particle.

While deriving the force $\mathbf{F}_{fp}$, the effect of fluid phase and of fluid core on the solid matrix have both to be included. The equation of motion for the lower part of the particle, as shown in inset (b) of Fig. 1, gives

$$\mathbf{F}_{fp} = -\mathbf{F}_{i,d} - \mathbf{F}_{o,d} + m_d\mathbf{a} + m_d\boldsymbol{\alpha} \times \mathbf{r}_d + m_d\omega^2 r_d \mathbf{e}_y \tag{16}$$

Here $\mathbf{F}_{i,d}$ and $\mathbf{F}_{o,d}$ are the hydrodynamic forces due to the fluid core and the fluid phase on the solid matrix [which can be obtained from Eq. (9)], m_d is the mass of the lower part of the particle, and $\mathbf{a}$, $\boldsymbol{\alpha}$ and ω are the acceleration, angular acceleration and angular velocity of the whole solid matrix, respectively. Finally, $\mathbf{r}_d$ is a vector pointing from the center of the particle to the center-of-mass of the lower part of the particle. The contribution of collisions and hydrodynamic interactions to the total shear stress is now given by $\tau_{pp} = \langle F^x_{pp}/A_p \rangle$ and $\tau_{fp} = \langle F^x_{fp}/A_p \rangle$.

4. RESULTS

A schematic illustration of the simulation setup is shown in Fig. 1. The suspension is placed between two moving solid walls oriented in the x direction and separated by a distance h. The walls move with speed u_w in opposite directions. Couette-flow conditions are thus created with the mean shear rate $\gamma = 2u_w/h$. Periodic boundary conditions were applied in the x direction. The simulation grid was rectangular and usually of size 128×128 lattice points. In some cases lattices of size 256×256 and even 384×384 lattice points were used. The diameter of particles was 10 lattice units and their density (including the solid matrix and the core fluid) was about 3.5 times the density of the carrier fluid. We chose this particular value for the density ratio as it is relevant for pigment suspensions used in paper coating.[34] As discussed in Sec. 2, the results we obtain are not sensitive to this value. Volume fraction (area fraction) of the particles was varied between $\langle \phi_s \rangle = 12\%$ and $\langle \phi_s \rangle = 52\%$. The shear Reynolds number $\mathrm{Re}_\gamma = \gamma d^2/\nu_f$, where d is the particle diameter and ν_f the kinematic viscosity of the carrier fluid, was varied between 0.14 and 11.7.

Simulations were started from a randomly distributed particle configuration with the fluid at rest (only walls moving). They were continued well beyond the point where a macroscopically stationary state was reached. Notice that the flow is always highly time dependent in the mesoscopic scale. The flow condition was monitored by computing the total shear stress at each simulation step. Whenever the value of the shear stress was adequately saturated at a constant value, the state of the system was supposed to be stationary. A typical duration of the macroscopically transient states was 200.000–600.000 simulation steps depending on the system size. The necessary time averaged quantities were calculated for the stationary states over 40.000 iteration steps, which even in the worst cases corresponded to several mean periods of a particle traversing the system. A snapshot of a typical numerical solution of a Couette flow of liquid-particle suspension in a macroscopically stationary state is shown in Fig. 1. The coloured contours indicate the viscous shear stress in the fluid phase.

Figure 2 shows the profiles of the average velocity U of the suspension, and the local volume fraction ϕ_s of the particles, between the moving plates in a macroscopically stationary flow for two systems with a different average volume fraction of particles. For each value of coordinate y, the average is taken over the surface $S(y)$, over a long period of time, and over an ensemble of three macroscopically identical systems. The average velocity is calculated for the local velocity field irrespective of the phase that occupies the location. The velocity U thus represents the "mixture velocity," i.e., the total flux of the suspension in the x direction.

For the relatively dilute suspension shown in Fig. 2a, the particles seem to concentrate near the center of the channel. Weak and somewhat diffuse layering may be observed near the walls. The velocity profile slightly deviates from linear and has a shallow S shape such that the shear rate is lower near the center. This can be understood on the basis of decreased particle concentration and, consequently, lower apparent viscosity near the walls. For the denser suspension shown in Fig. 2b, the most spectacular phenomenon is the strong layering of particles near the walls. Weaker layering is visible even in the central region of the channel. Notice that such layering was also observed in light-diffraction experiments by Hoffman.[35] The shear rate oscillates strongly near the walls, and the velocity profile seems to have features of slippage at the walls. At the central part, the shear rate is clearly lower than the average value (indicated by the slope of the dashed line).

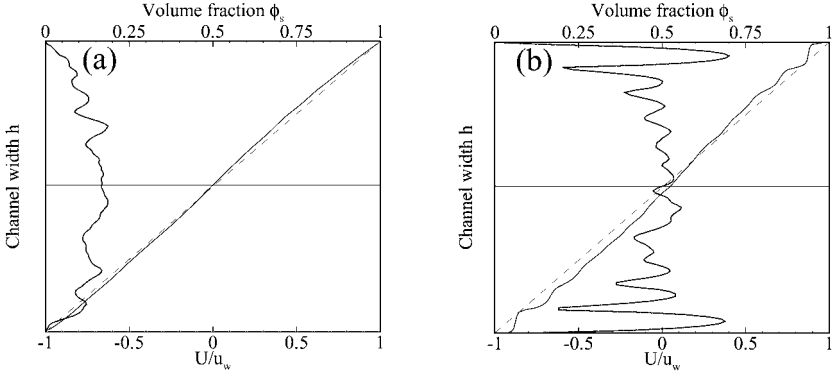

Fig. 2. The volume fraction of particles and the mean velocity profile of the suspension across the channel width h for a suspension with mean solid volume fractions $\langle\phi_s\rangle = 12\%$ (a) and $\langle\phi_s\rangle = 48\%$ (b). Thick solid line indicates the volume fraction, and thin solid line is the suspension velocity divided by the velocity of the wall. Dashed line represents a linear velocity profile.

It is evident from Figs. 2 that the mean flow of the suspension is strongly affected by the underlying two-phase nature of the fluid. It is however instructive to first treat the suspension as a non-Newtonian single-phase fluid, and compute its apparent viscosity, as would be measured in an appropriate viscometric experiment. In Table I we show the relative contributions of the four different momentum transport mechanisms, presented in Eq. (11), for two averaged solid volume fractions $\langle\phi_s\rangle$. The convective (pseudo-turbulent) stresses are very small as compared to the other stress terms, and will not be considered in the following.

Figure 3a shows the relative apparent viscosity μ_s/μ_f as a function of the average solid volume fraction $\langle\phi_s\rangle$ for various values of the shear Reynolds number Re_γ. Here μ_f is the viscosity of the carrier fluid and the apparent viscosity of the suspension is defined as $\mu_s = \tau_T/\gamma$, where τ_T is the total shear stress on the moving walls, and γ is the mean shear rate given by the velocity difference and the distance between the two moving walls. Also shown in Fig. 3a is the result by Krieger and Dougherty,[36] which is applicable at low Reynolds numbers for both two- and three-dimensional suspensions. According to that result

$$\mu_s/\mu_f = (1-\langle\phi_s\rangle/\phi_{\max})^{-[\eta]\,\phi_{\max}} \tag{17}$$

where $\langle\phi_s\rangle$ is the averaged solid volume fraction and $\phi_{\max}$ is the maximum packing fraction at which viscosity diverges. The factor η is the intrinsic viscosity of the suspension, which varies between 2.50 and 2.67 for rigid spheres depending on whether the particles are charged or not. Experimental results of Van Der Werff and De Kruif[37] suggest $[\eta]\,\phi_{\max} = 2$. In Fig. 3b we show the calculated values of the relative viscosity for $\mathrm{Re}_\gamma = 0.1$ and 1.5 as functions of scaled volume fraction $\langle\phi_s\rangle/\phi_{\max}$ together with a number of previous experimental and numerical results, all obtained for Reynolds numbers $\mathrm{Re}_\gamma < 1$. The numerical results included in Fig. 3b are

Table I. Relative Contribution of Different Momentum Transfer Mechanisms to the Total Shear Stress τ_T for Two Different Values of Average Solid Volume Fraction (%). Stresses σ_f and σ_s Are the Pseudo-Turbulent Stresses of the Fluid and Solid Phases, Respectively, τ_f Is the Viscous Stress of the Fluid Phase, and τ_s Is the Solid Stress (Internal Shear Stress in the Suspended Particles)

$\langle\phi_s\rangle$	σ_f/τ_T	σ_s/τ_T	τ_f/τ_T	τ_s/τ_T
12%	0.013	0.057	73.98	26.03
52%	0.083	0.196	11.30	88.33

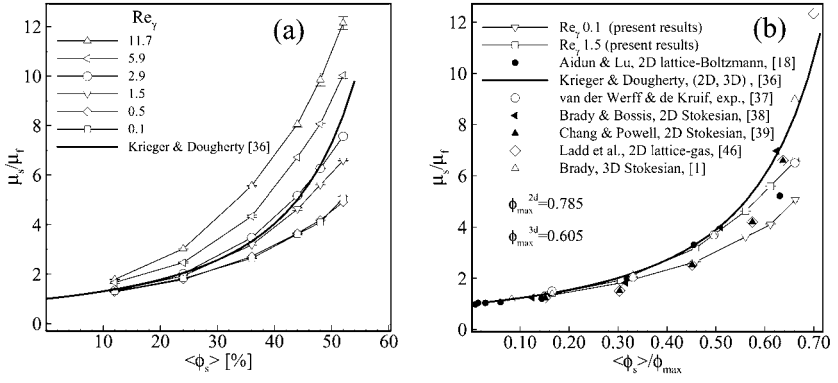

Fig. 3. (a) The calculated apparent relative viscosity μ_s/μ_f as a function of the average solid volume fraction $\langle\phi_s\rangle$ for various values of shear Reynolds number Re_γ. Also shown is the semiemperical result by Krieger and Dougherty [see Eq. (17)]. The error bars indicate the maximum statistical variation obtained for a number of macroscopically identical systems. (b) Comparison of the calculated relative viscosity with previous experimental and numerical results at small Reynolds numbers, for 2D and 3D systems. The solid volume fractions have been normalized by the maximum flowing fraction, $\phi_{\max}^{2d} = 0.785$ (simple cubic packing) and $\phi_{\max}^{3d} = 0.605$ (hexagonal packing) in order to allow for comparison of two- and three-dimensional results.

obtained using Stokesian approximation, lattice-gas simulations, or lattice-Boltzmann simulations, for both two-dimensional and three-dimensional systems. The values of the maximum packing ratio $\phi_{\max}$ used in scaling the volume fraction are 0.785 (2D) and 0.605 (3D), which correspond to "flowing" arrangements of simple cubic and hexagonal packing perpendicular to the plane of shear, respectively.[37–39] It is evident from Fig. 3b that the results obtained here agree very well with the previous results shown. In Fig. 4, the same data as in Fig. 3a is shown as a function of the shear Reynolds number, i.e., the dimensionless mean shear rate, for various values of the solid volume fraction. As is evident from Fig. 4, viscosity increases with increasing volume fraction of the particles in accordance with the Krieger and Dougherty result, and clear shear thickening is found. These effects are in good qualitative agreement with the observed behaviour of many concentrated suspensions.[35, 40] Also the simulation result of ref. 41 for very low Reynolds numbers when Brownian motion dominates (see the inset in Fig. 4), agrees with present results.

Having studied the bulk properties of the suspension, it is now instructive to take notice of the actual two-phase structure of the fluid, and compute the contribution of the two phases to the total shear stress (or the apparent viscosity). In Fig. 5 shown is the ratio of the shear stress carried by the fluid, τ_f, and the shear stress carried by particles, τ_s, to the total

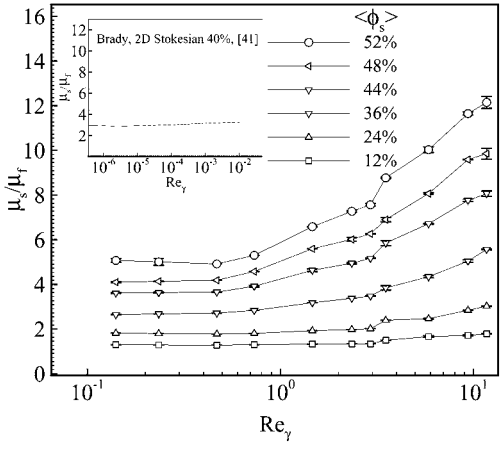

Fig. 4. Relative viscosity μ_s/μ_f as a function of shear Reynolds number Re_γ for different mean solid volume fractions $\langle\phi_s\rangle$. The simulation result of ref. 41 for very low Reynolds numbers is shown in the inset.

shear stress as a function of the Reynolds number Re_γ. Figures 5a and 5b show the results for the solid volume fraction $\langle\phi_s\rangle = 12\%$ and $\langle\phi_s\rangle = 48\%$, respectively. Figure 6 shows the same ratio as a function of the average solid volume fraction at a fixed Reynolds number $\mathrm{Re}_\gamma \approx 3$. As evidenced by Fig. 6, the contribution of the solid phase to the total shear stress strongly increases with the solid volume fraction. Within our two-dimensional model fluid, particles carry almost 90% of the total shear stress already at $\langle\phi_s\rangle = 50\%$. Less obvious is the behaviour of the relative contributions of the two phases as functions of the shear rate. As shown in Fig. 5, the relative shear stress of the solid phase (and consequently, of the fluid phase) is

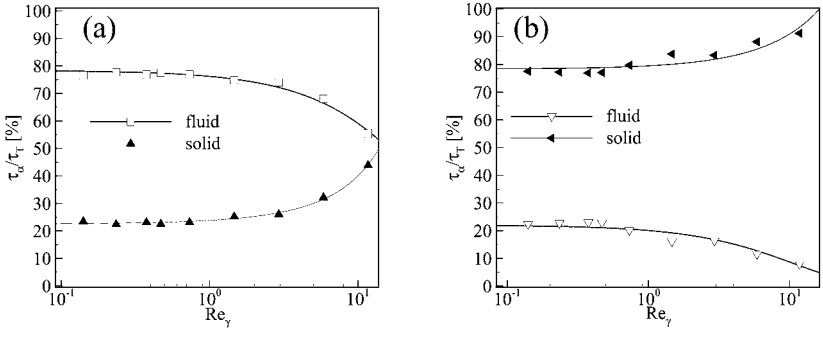

Fig. 5. The ratios of viscous stress τ_f and solid stress τ_s to the total shear stress τ_T as functions of the shear Reynolds number Re_γ, for a suspension with $\langle\phi_s\rangle = 12\%$ (a), and for a suspension with $\langle\phi_s\rangle = 48\%$ (b).

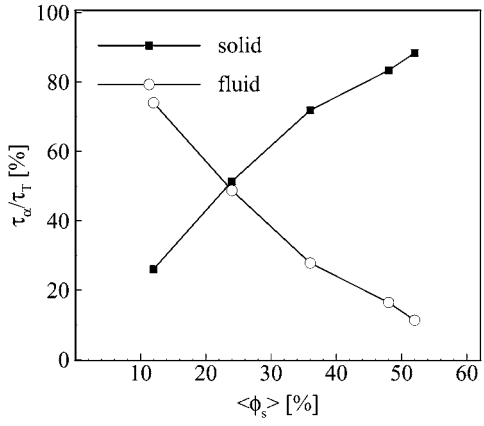

Fig. 6. The ratios of viscous stress τ_f and solid stress τ_s to the total shear stress τ_T as functions of the average solid volume fraction $\langle \phi_s \rangle$ for $\mathrm{Re}_\gamma \approx 3$.

nearly independent of Re_γ at low Reynolds numbers, but begins to increase with Reynolds number increasing beyond unity. Comparing with Fig. 4, one is tempted to conjecture that this phenomenon is related to shear thickening. While the detailed mechanism responsible for this phenomenon is still somewhat unclear, preliminary results indicate that it is related to mesoscopic processes such as clustering[42] and layering of particles. This interesting topic will be discussed in more detail elsewhere.

5. CONCLUSIONS

We have studied the two-dimensional laminar Couette flow of a liquid-particle suspension using direct numerical simulations. The results indicate that the lattice-Boltzmann method used in these simulations produces a physically plausible solution to the complicated time-dependent flow of the carrier liquid with freely moving suspended particles. According to the results obtained, a non-uniform concentration profile and even a layered structure of particles appear near the moving solid walls. In real fluids, as also indicated by some experiments, such phenomena may distort the interpretation of results of viscometric measurements.[43] The overall rheological behaviour of the modeled suspension is dilatant, and is in a qualitative agreement with the behaviour observed for real suspensions with hard spherical particles suspended in a simple Newtonian liquid.[44, 45] The shear-thickening behaviour seems to be related to the enhanced relative contribution of the solid phase in the total shear stress as the shear rate is increased. The exact particle-scale mechanisms leading to this phenomenon remain to be analyzed in more detail.

The numerical method applied here can thus be used to qualitatively study the mechanisms that contribute to the intricate rheology of particulate suspensions. Simulations can also help better understand and interpret experimental viscometric measurements. For quantitatively accurate results, three-dimensional simulations and more realistic modeling of particle–particle interactions may be required.

ACKNOWLEDGMENTS

Financial support from the Technology Development Centre (Finland) and the Academy of Finland (project no. 44875) is gratefully acknowledged.

REFERENCES

1. J. F. Brady, The rheological behaviour of concentrated colloidal dispersions, *J. Chem. Phys.* **99**:567 (1993).
2. T. N. Phung, J. F. Brady, and G. Bossis, Stokesian dynamics simulation of Brownian suspensions, *J. Fluid Mech.* **313**:181 (1996).
3. R. W. Whorlow, *Rheological Techniques*, 2nd ed. (Ellis Horwood, Great Britain, 1992).
4. S. L. Soo, *Multiphase Fluid Dynamics* (Science Press, Beijing, 1990).
5. D. Qi, Lattice-Boltzmann simulations of particles in non-zero-Reynolds-number flows, *J. Fluid Mech.* **385**:41 (1999).
6. G. Segré and A. Silberberg, Behaviour of macroscopic rigid spheres in Poiseuille flow, Part 2, Experimental results and interpretation, *J. Fluid Mech.* **14**:136 (1962).
7. G. P. Krishnan and D. T. Leighton, Inertial lift on a moving sphere in contact with a plane wall in a shear flow, *Phys. Fluids* **7**:2538 (1995).
8. C. K. Aidun, Y. N. Lu, and E. J. Ding, Direct analysis of particulate suspensions with inertia using the discrete Boltzmann equation, *J. Fluid Mech.* **373**:287 (1998).
9. S. Chen and G. Doolen, Lattice-Boltzmann method for fluid flows, *Ann. Rev. Fluid Mech.* **30**:329 (1998).
10. B. Chopard, P. O. Luthi, and J. F. Wagen, A Lattice-Boltzmann method for wave propagation in urban microcells, *IEE Proc.-Microw. Antennas Propagation* **144**:251 (1997).
11. J. M. Buick, C. A. Greated, and D. M. Campbell, Lattice BGK simulation of sound waves, *Europhys. Lett.* **43**:235 (1998).
12. X. W. Shan and G. Doolen, Diffusion in a multicomponent lattice-Boltzmann equation model, *Phys. Rev. E* **54**:3614 (1996).
13. S. Succi and R. Benzi, Lattice-Boltzmann equation for quantum-mechanics, *Physica D* **69**:327 (1993).
14. X. W. Shan and H. D. Chen, Lattice-Boltzmann model for simulating flows with multiple phases and components, *Phys. Rev. E* **47**:1815 (1993).
15. A. J. Wagner and J. M. Yeomans, Spinodal decomposition in two-dimensional binary fluids, *Int. J. Mod. Phys. C* **9**:1373 (1998).
16. E. Aharonov and D. H. Rothman, Non-Newtonian flow (through porous media): A lattice-Boltzmann method, *Geophys. Res. Lett.* **20**:679 (1993).
17. F. J. Alexander, H. Chen, S. Chen, and G. D. Doolen, Lattice-Boltzmann model for compressible fluids, *Phys. Rev. A* **46**:1967 (1992).
18. C. K. Aidun and Y. Lu, Lattice-Boltzmann simulation of solid particles suspended in a fluid, *J. Statist. Phys.* **81**:49 (1995).

19. A. J. C. Ladd, Short-time motion of colloidal particles: Numerical simulation via a fluctuating lattice-Boltzmann equation, *Phys. Rev. Lett.* **70**:1339 (1993).
20. H. Chen, S. Chen, and W. H. Matthaeus, Recovery of the Navier–Stokes equations using a lattice-gas Boltzmann method, *Phys. Rev. A* **45**:R5339 (1992).
21. G. R. McNamara and G. Zanetti, Use of the Boltzmann equation to simulate lattice-gas automata, *Phys. Rev. Lett.* **61**:2332 (1988).
22. Y. H. Qian, D. d'Humières, and P. Lallemand, Lattice BGK for Navier–Stokes equation, *Europhys. Lett.* **17**:479 (1992).
23. O. Behrend, R. Harris, and P. B. Warren, Hydrodynamic behaviour of lattice-Boltzmann and lattice Bhatnagar–Gross–Krook models, *Phys. Rev. E* **50**:4586 (1994).
24. A. J. C. Ladd, Numerical simulations of particulate suspensions via a discretized Boltzmann equation. Part 1. Theoretical foundation, *J. Fluid Mech.* **271**:285 (1994).
25. A. J. C. Ladd, Numerical simulations of particulate suspensions via a discretized Boltzmann equation. Part 2. Numerical results, *J. Fluid Mech.* **271**:311 (1994).
26. O. Behrend, Solid-fluid boundaries in particle suspension simulations via the lattice Boltzmann method, *Phys. Rev. E* **52**:1164 (1995).
27. A. J. C. Ladd and R. Verberg, Lattice-Boltzmann simulations of particle-fluid suspensions, *J. Statist. Phys.* **104**:1191 (2001).
28. P. Raiskinmäki, A. Shakib-Manesh, A. Koponen, A. Jäsberg, M. Kataja, and J. Timonen, Simulation of non-spherical particles suspended in a shear flow, *Comp. Phys. Comm.* **129**:185 (2000).
29. A. J. C. Ladd, Sedimentation of homogeneous suspensions of non-Brownian spheres, *Phys. Fluids* **9**:491 (1997).
30. D. I. Dratler, W. R. Schowalter, and R. L. Hoffman, Dynamic simulation of shear thickening in concentrated colloidal suspension, *J. Fluid Mech.* **353**:1 (1997).
31. J. Feng, H. H. Hu, and D. D. Joseph, Direct simulation of initial-value problems for the motion of solid bodies in a Newtonian fluid. 1. Sedimentation, *J. Fluid Mech.* **261**:95 (1994).
32. http://www.phys.jyu.fi/homepages/amir/test.html.
33. L. D. Landau and E. M. Lifshitz, *Theory of elasticity*, 3rd ed. (Pergamon Press, 1986).
34. *Pigment coating and surface sizing of paper*, *Papermaking Science and Technology*, Vol. 11, E. Lehtinen, ed. (Fapet Oy, Jyväskylä, Finland, 2000).
35. R. L. Hoffman, Explanations for the cause of shear thickening in concentrated colloidal suspensions, *J. Rheol.* **42**:111 (1998).
36. I. M. Krieger and T. J. Dougherty, A mechanism for non-Newtonian flow in suspensions of rigid spheres, *Trans. Soc. Rheol.* **3**:137 (1959); I. M. Krieger, Rheology of monodisperse lattices, *Adv. Colloid Interface Sci.* **3**:111 (1972).
37. J. C. van der Werff and C. G. de Kruif, Hard-sphere colloidal dispersions: The scaling of rheological properties with particle size, volume fraction and shear rate, *J. Rheol.* **33**:421 (1989).
38. J. F. Brady and G. Bossis, The rheology of concentrated suspensions of spheres in simple shear flow by numerical simulation, *J. Fluid Mech.* **155**:105 (1985).
39. C. Chang and R. L. Powell, Dynamic simulation of bimodal suspensions of hydrodynamically interacting spherical particles, *J. Fluid Mech.* **253**:1 (1993).
40. W. J. Frith, P. d'Haene, R. Buscall, and J. Mewis, Shear thickening in model suspensions of sterically stabilized particles, *J. Rheol.* **40**:531 (1996).
41. J. F. Brady and G. Bossis, Stokesian dynamics, *Ann. Rev. Fluid Mech.* **20**:111 (1988).
42. P. Raiskinmäki *et al.*, to be published.

43. J. H. C. Luke, Decay of velocity fluctuations in a stably stratified suspension, *Phys. Fluids.* **12**:1619 (2000).
44. L. Bergström, Shear thinning and shear thickening of concentrated ceramic suspensions, *Coll. Surf. A* **133**:151 (1998).
45. B. van der Vorst, D. van den Ende, N. J. J. Aelmans, and J. Mellema, Shear viscosity of an ordering latex suspension, *Phys. Rev. E* **56**:3119 (1997).
46. A. J. C. Ladd, M. E. Colvin, and D. Frenkel, Application of lattice-gas cellular automata to the Brownian motion of solids in suspension, *Phys. Rev. Lett.* **60**:975 (1988).